

A simple network-based model for simulating the Syrian 2011-2024 civil war

KONSTANTINOS TOPALOGLOU¹ AND RICCARDO MARCHESE¹

¹ University of Bologna

ABSTRACT

We formulate a simple model for simulating the dynamics of an armed conflict with respect to the exchange of populated grounds between the involved parties. The model is applied to the later stage of the 2011-2024 Syrian civil war. A geographical network of catalogued Syrian cities is taken as the stage whereupon the conflict is evolved from the initial state of March 2019 with a decision- and battle-making algorithm for each node against its rival neighbours. The data utilised in the decision-making process and the troop layout of the parties includes the geographical distance between nodes, the population, the vicinity to oil and gas resources and related infrastructure, the dominant ethnic or religious group, as well as network-related measures that reveal the strategic value of the network's nodes. We assess the weight of the aforementioned parameters and the decision making process that appear to best reproduce the sudden takeover of the state-held grounds by rebel groups that took place in December 2024, signaling the end of the Bashar al-Assad regime in Syria.

1. INTRODUCTION

The Syrian civil war, which erupted in 2011 and extended through 2024, stands as one of the most enduring conflicts of the modern era. Characterized by shifting alliances, ethnoreligious fragmentation, and foreign interventions, the war has led to dramatic changes in territorial control and inflicted profound humanitarian consequences. Despite the availability of historical data and visual documentation, predictive modelling of the conflict's territorial dynamics remains a challenge due to the interplay of demographic, geographic, and strategic factors.

In this work, we propose a network-based simulation framework to model the evolution of territorial control during the later stages of the Syrian civil war. Our approach treats Syrian cities and towns as nodes in a geographical network, each enriched with attributes such as population size, dominant ethnoreligious identity, proximity to oil and gas infrastructure, and network centrality measures. The simulation evolves from an initial occupation through iterative troop allocation, probabilistic battle outcomes, and memory-based reinforcement dynamics.

The key point of this work lies in the dual use of network centrality metrics. These measures guide both the redistribution of troops and the selection of strategic targets, reflecting the dual priorities of logistical feasibility and symbolic or tactical importance. Furthermore, we introduce stochasticity in target selection and inertia in troop evolution, enhancing the realism of the simulation. A structural collapse mechanism is also implemented to mimic the fragmentation and retreat of overstretched factions, particularly the Assad-led State forces.

By calibrating the model to reproduce the December 2024 rebel takeover, we aim to assess the relative influence of demographic, geographic, and strategic parameters in shaping the outcome of the Syrian conflict. Our results offer insights into how local node-level attributes can drive macro-level shifts in territorial control, and how network-aware modelling can illuminate the dynamics of modern warfare.

2. MODEL SETUP

The geographical network is constructed upon a catalogue of 8010 Syrian populated towns which are taken to serve as nodes, labelled with longitude-latitude coordinates x_i, y_i . The node-node distance

$$d_{ij} = \sqrt{\cos^2\left(\frac{y_i + y_j}{2}\right)(x_i - x_j)^2 + (y_i - y_j)^2} \quad (1)$$

provides the weighted edges for the network so long as it does not exceed a threshold value d_0 .

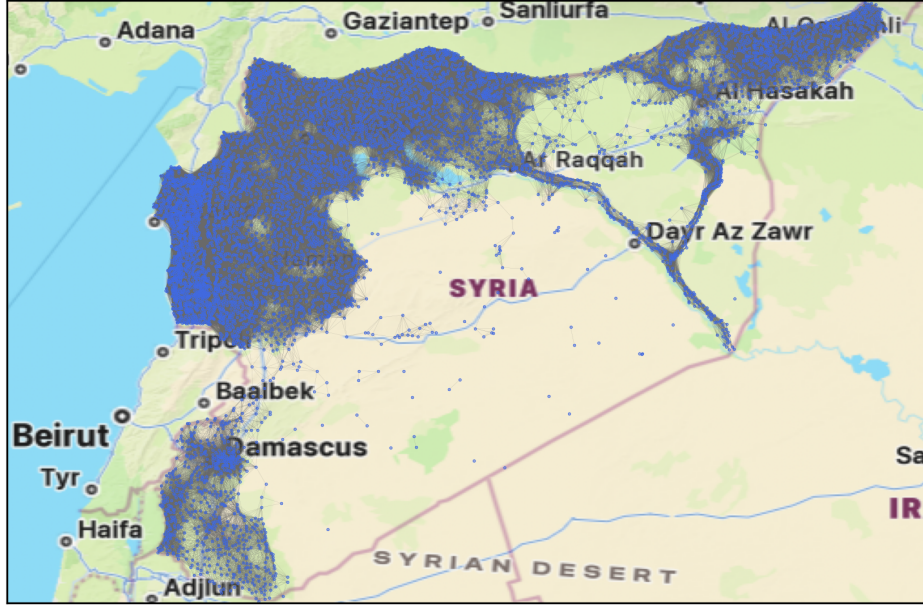


Figure 1. Geographical network of Syrian cities catalogued by HOT (1). The network edges are assigned the node-node geographical distance as a weight or are nullified if the distance exceeds a threshold $d_0 = 0.1$.

Each node is assigned a set of characterising quantities that determine its value as a target and its dynamical properties. These are the following:

1. Population (*pop*, integer): The population of the city, or otherwise populated region, represented by the node;
2. Dominant ethnic or religious group (*ethn*, label): the dominant group within the node's population as given by broader regional data, out of the three options *alawites*, *sunni*, *kurds*;
3. Oilscore (*os*, number): the distance to the closest region marked as possessing oil reserves, natural gas reserves, or relevant industrial infrastructure;
4. Betweenness centrality (*bce*, number): The network's unweighted betweenness centrality measure for the given node;
5. Closeness centrality (*cce*, number): the network's unweighted closeness centrality measure for the given node;
6. Eigenvector centrality (*eig*, number): the normalized eigenvector centrality measure of node in the largest, connected, network component;
7. Fiedler value (*fiedler*, number): the Fiedler value, or algebraic connectivity, of the three ethnic or religious groups.

2.1. Simulation algorithm

The goal of the simulation is to evolve an input initial occupation state, such that every node is furthermore assigned an initial occupier out of the three parties *State* (representing Bashar al-Assad's army of the Syrian state), *Sunni* (an amalgamation of the various rebel groups that shared a Sunni Muslim identity, including the HTS) and *Kurds* (rebels groups of Kurdish identity, including the YPG). Subsequent occupation states which are produced in each of N total iterations thus track the exchange of populated grounds among these three parties.

Each iteration of the simulation consists of two stages: *preparation* and *battle*. During the *preparation* stage each node is assigned a number of troops n_i anew based on the formula

$$n_i = 0.01(\text{pop}_i + 100)(1 + 0.5(\eta_m - 0.5)) \quad (2)$$

where the quantity

$$\eta_m = \begin{cases} 1 & \text{if } occ_i = ethn_i \\ 0 & \text{else} \end{cases} \quad (3)$$

and occ_i labels the node with its current occupying party.

In the *battle* stage, for every node i , we isolate the neighbours j whose occupier is a rival party, and compute a probability-like quantity P_{ij} meant to signify the value as a potential target. This is put together by the individual contributions of each of the model's parameters:

$$\begin{aligned} p_{pop,ij} &= \frac{2}{\pi} \arctan(c_{pop} \cdot pop_j + \epsilon_{dist}), \\ p_{os,ij} &= 1 - \frac{2}{\pi} \arctan(c_{os} \cdot os_j), \\ p_{dis,ij} &= 1 - \frac{2}{\pi} \arctan(c_{dist} \cdot d_{ij}), \\ p_{dam,ij} &= 1 - \frac{2}{\pi} \arctan(c_{dam} \cdot d_j^{dam}), \end{aligned} \quad (4)$$

as well as those obtained by network measures

$$\begin{aligned} p_{bce,ij} &= \frac{2}{\pi} \arctan(c_{bce} \cdot bce_j) \\ p_{cce,ij} &= \frac{2}{\pi} \arctan(c_{cce} \cdot cce_j), \\ p_{eig,ij} &= eig_j, \end{aligned} \quad (5)$$

where d_{ij} is the adjacency-based distance, d_j^{dam} is the distance of node j from Damascus, and the remaining quantities correspond to node-level attributes and network centralities. The manner in which these contributions are combined is meant to reflect the decision-making approach of the parties. We distinguish four different possibilities (out of, in principle, several others) utilising a logical AND and OR combination rule for the probabilities:

- ... AND ... AND ... :

$$p_{ij} = p_{pop,ij} \cdot p_{os,ij} \cdot p_{dis,ij}$$

- ... AND (... OR ...) :

$$p_{ij} = p_{pop,ij} \cdot (p_{os,ij} + p_{dis,ij} - p_{os,ij}p_{dis,ij})$$

- (... OR ...) AND ... :

$$p_{ij} = (p_{pop,ij} + p_{os,ij} - p_{pop,ij}p_{os,ij}) \cdot p_{dis,ij}$$

- ... OR ... OR ... :

$$p_{pop-os,ij} = p_{pop,ij} + p_{os,ij} - p_{pop,ij}p_{os,ij},$$

$$p_{ij} = p_{pop-os,ij} + p_{dis,ij} - p_{pop-os,ij}p_{dis,ij}.$$

and the result is lastly combined with a logical OR to the Damascus distance component

$$p_{ij} \rightarrow p_{ij} + p_{dam,ij} - p_{ij}p_{dam,ij}.$$

and with a logical OR to one of the centralities measures of the network:

$$\begin{aligned} P_{ij} &= p_{ij} + p_{bce,ij} - p_{ij} \cdot p_{bce,ij}, \\ P_{ij} &= p_{ij} + p_{cce,ij} - p_{ij} \cdot p_{cce,ij}, \\ P_{ij} &= p_{ij} + p_{eig,ij} - p_{ij} \cdot p_{eig,ij}. \end{aligned}$$

The combination of probabilities may in principle be made more intricate by utilising more of the available measures by using AND and OR operations.

The probability is then given a boost depending on whether the ethnic identity of the attacking node matches that of the potential target:

$$P_{ij} \rightarrow \begin{cases} 1 - \frac{1 - P_{ij}}{c_{ethn}} & \text{if } occ_i = ethn_j \\ P_{ij} & \text{else.} \end{cases} \quad (6)$$

The constants $c_{pop}, c_{os}, c_{dist}, c_{bce}, c_{ethn}, \epsilon_{dist}$ are parameters of the model and are mostly fixed by requiring that an extremal value of the dataset attains a desired probability, i.e. that the highest catalogued population in pop is assigned a value $p_{pop} = 0.99$.

Following the calculation of P_{ij} for all rival neighbours, the attacking node i picks the target j which has the highest P_{ij} and performs a battle, mobilising a number of troops equal to $N_i = n_i \cdot P_{ij}$. The battle is

- won, if $N_i \geq n_j$: the occupation label of node j then changes to the label of i , and $n_j \rightarrow N_i - n_j$,
- lost, if $N_i < n_j$: the occupation remains unchanged, and $n_j \rightarrow n_j - N_i$,

while the attacker loses the strength they mobilised, $n_i \rightarrow n_i - N_i$.

2.2. Memory-Based Simulation and Stochastic Target Selection p

In this subsection we present two modifications to the simulation algorithm, extending our previous model by applying a stochastic approach to target selection, and a memory-retaining method of coordinating troop movements. To avoid repetition, we now focus on the new ingredients of the model.

A key novelty of the model is the introduction of a stochastic *memory-based movement* of troops. In the *battle* stage, for every node i we first isolate its rival neighbours j (those with a different occupier) and compute an attractiveness score P_{ij} as a combination of the model's demographic, geographic and network parameters, as discussed in 2.1. A deliberate design choice in the model is the use of similar network-based metrics - such as eigenvector centrality, closeness, and betweenness-in both the troop redistribution kernel T_{ij} and the target attractiveness score P_{ij} . While this may appear redundant at first glance, the rationale lies in the distinct roles these components play in the simulation.

A kernel T_{ij} governs the redistribution of continuous troop resources across the network. Here, centrality metrics serve to bias movement toward structurally important nodes, reflecting logistical ease, connectivity, and strategic depth. For example, nodes with high closeness centrality are more accessible and thus more likely to receive reinforcements, while nodes with high betweenness act as transit hubs, facilitating flow across the network.

In contrast, the score P_{ij} is used to construct a probability distribution over rival targets for attack selection, which is performed stochastically, in the stead of going for the target of maximal P as before. In this context, the metrics employed reflect strategic desirability rather than logistical accessibility. A node with high eigenvector centrality may be targeted not because it is easy to reach, but because it is influential or symbolically important within the network.

By using the same metrics in both contexts but with different interpretations and weightings, the model captures a realistic duality: factions tend to reinforce well-connected areas while simultaneously seeking to conquer strategically valuable ones. This dual use enhances the coherence of the simulation, ensuring that both movement and aggression are informed by the underlying network structure, albeit in semantically distinct ways.

The attractiveness score matrix P_{ij} is calculated as in the previous paragraph, ultimately using the result of equation 6 or some variant thereof depending on one's choice of model. Independently, a transition weight is computed from geographic ease and network centralities:

$$T_{ij} = \frac{e^{-d_{ij}}(1 + \alpha eig_j)(1 + \beta cce_j)}{\sum_{k \in \mathcal{N}(i)} e^{-d_{ik}}(1 + \alpha eig_k)(1 + \beta cce_k)}, \quad (7)$$

which represents the intrinsic movement propensity from node i to j . For rival targets j we defined an attack probability distribution, which is then straightforwardly defined as:

$$p_{ij}^{\text{attack}} = \frac{P_{ij}}{\sum_k P_{ik}}, \quad (8)$$

which controls the stochastic choice of the target.

A target J is sampled according to p_{ij}^{attack} , but the number of troops deployed scales with the *unnormalised* score P_{ij} :

$$N_i = n_i \cdot P_{ij}.$$

This distinction preserves randomness in target selection while allowing the intensity of the attack to grow with the raw attractiveness of the target.

After all planned attacks are collected, troops diffuse according to the transition matrix:

$$\mathbf{moved} = T^\top \mathbf{n}, \quad \mathbf{n} \leftarrow (1 - 0.3) \mathbf{n} + 0.3 \cdot \mathbf{moved}. \quad (9)$$

Battles are then resolved sequentially:

- **Success:** if $N_i \geq n_J$, node J is conquered and its troop level set to $n_J \rightarrow N_i - n_J$.
- **Failure:** if $N_i < n_J$, node J resists but loses $n_J \rightarrow n_J - N_i$.
- In all cases, the attacker loses the deployed troops $n_i \rightarrow n_i - N_i$.

At each iteration N , new recruitment levels \mathbf{n}_{new} are computed afresh from the current occupation state without Fiedler corrections. Rather than replacing the previous troop vector outright, we blend the new and old values to obtain the current charges:

$$\mathbf{n}_{t+1}^{\text{pre}} = 0.999 \mathbf{n}_t + 0.001 \mathbf{n}_{\text{new}}. \quad (10)$$

This weighted update introduces “inertia” into the model: troop strengths evolve gradually rather than instantaneously, mimicking the lag inherent in recruitment, logistics, and redeployment. In other words, each node retains 99.9% of its previous troop level and only 0.1% of the newly computed level is added per time step. This approach ensures that troop levels have memory of the past, but can still adapt to new recruitment trends, yielding smoother and more realistic temporal dynamics compared to a purely instantaneous update.

The updated troop vector $\mathbf{n}_{t+1}^{\text{pre}}$ is then passed to the main simulation step, which performs a redistribution, stochastic attack selection and battle resolution. Finally, the new occupation state is recorded, and the cycle repeats for N total iterations.

This framework ensures that the evolution of occupation and troop strength is both stochastic and network-aware. It reproduces strategic tendencies observed in the conflict, such as preference for nodes closer to Damascus, avoidance of overextension into distant or ethnically different territories, and reinforcement of well-connected clusters. Because all four stages interact dynamically, factions that become topologically fragmented gradually lose cohesion and recruiting power, while strongly connected areas tend to persist or grow over time.

2.3. Fiedler-based initialisation

To initialise the simulation, the initial occupation state is obtained from the data and its troop levels per node are computed once including Fiedler-based corrections, which yields the starting distribution of military strength over the three factions. Each node i is associated with an occupier faction $f_i \in \{\text{state}, \text{sunni}, \text{kurds}\}$. A multiplicative factor $\text{mul}_{\text{faction}}$ may then be additionally applied, to provide a scaling determined by the Fiedler value f_{faction} of the factional subgraph. Consequently, at the initialization, the troop strength n_i computed via equation 2 is further modulated as

$$n_i \rightarrow n_i \frac{f_{\text{faction}(i)}}{f_{\max}}, \quad (11)$$

where $f_{\max} = \max \{f_{\text{state}}, f_{\text{sunni}}, f_{\text{kurds}}\}$, so that factions with more weakly connected territories (*lower* Fiedler value) start with proportionally lower effective strength. This approach yields initial conditions in which demographic capacity, ethnic alignment, and structural connectivity jointly determine the baseline troop strength for each node.

2.4. Structural collapse

Another - biased - addition was made in the code, after analysing the historical events, it was decided to mimic the retreat of the Assad army. At the end of each iteration we perform a *structural collapse check* designed to mimic the progressive weakening of an overstretched or fragmented faction. The procedure evaluates the total network centrality of the nodes held by the *State* faction:

$$C_{\text{State}} = \sum_{i \in \mathcal{S}_{\text{State}}} (eig_i + bce_i + cce_i), \quad (12)$$

and compares it to the centrality lost to rival factions:

$$C_{\text{lost}} = \sum_{i \notin \mathcal{S}_{\text{State}}} (eig_i + bce_i + cce_i). \quad (13)$$

If the relative loss exceeds a threshold,

$$\frac{C_{\text{lost}}}{C_{\text{State}}} > \theta_{\text{loss}}, \quad (14)$$

the remaining *State* nodes suffer a multiplicative reduction of their troop strengths. This reduction is spatially biased: nodes farther from Damascus incur a stronger penalty,

$$n_i \rightarrow n_i \max(0.2, 1 - \delta - \kappa d_i^{\text{Dam}}), \quad i \in \mathcal{S}_{\text{State}}, \quad (15)$$

where d_i^{Dam} is the distance from Damascus and δ, κ are decay parameters ensuring that no node falls below a fixed minimum fraction of its troops.

In this way the algorithm captures a realistic effect whereby a faction that has lost a critical mass of strategically important territory undergoes a rapid, network-wide weakening — especially in its more peripheral holdings — reflecting breakdown of logistics, morale and communication.

3. DATA

The necessary data for quantifying this model, involving various aspects of the Syrian war and civil landscape, has been scarce and in some cases obtained with unorthodox methods. In this section we provide the sources of the relevant data and illustrate the process used to incorporate them into this simulation. This includes data for catalogued cities and population (1), oil and gas reserves and infrastructure (2; 5), ethnic & religious groups per region (3; 4), and the state of occupation during March of 2019, taken as an initial state for the simulation.

3.1. Populated regions

We implement the data catalogued in the dataset [Syria Populated Places](#) by the Humanitarian OpenStreetMap Team, utilising 8010 of the total 8995 places (including ‘isolated dwelling’, ‘town’, ‘village’, ‘hamlet’, ‘city’) as having adequate information. We highlight the note by the contributors that the data is gathered by “volunteered geographic information” and that “OpenStreetMap data is crowd sourced and cannot be considered to be exhaustive”.

3.2. Oil & natural gas locations

For the purposes of assigning a score to Syrian towns based on their proximity to resources and infrastructure, we manually identify locations on the map which are documented as hosting oil reserves, gas reserves, or important stations for the processing of said resources. These are obtained from maps presented in (2; 5) by the Energy Consulting Group website and an article by Brenda Shaffer on behalf of the Atlantic Council.

3.3. Ethnoreligious groups

In a similar fashion as in the previous section we locate manually the regions on the map which are dominated by one of the following groups: Sunni Muslims, Alawite Muslims and Kurds. The map is therefore divided in regions associated to one of these three identities and all nodes contained in a region are assigned the respective identity. Maps and relevant information are provided in (4; 3) as well as a map in Wikimedia Commons “[Syria Ethnoreligious Map](#)”.

An important point to be made here is that this procedure is considerably inaccurate with regards to both the rough treatment of the data itself and the overlooking of minority groups and groups that don’t belong to our classification scheme. Essentially we deem the dominant group as representative of the node’s entire population, disregarding the relative size of smaller minorities which, realistically, coexist in the same region, as we could not find reliable and consistent data for the entirety of Syria which documents minority groups and the percentage of the population that they make up. An exception to this statement is a collection of nodes bordering at least two regions, where an overlap of identities is deliberately permitted. Additionally we ignore the presence of other groups, which may be dominant in other, smaller regions - one such example is the Druse-dominated south edge of Syria, which, partly due to the stance of neutrality that it tried to maintain throughout the war, is ultimately considered of lower importance in our highly approximate model.

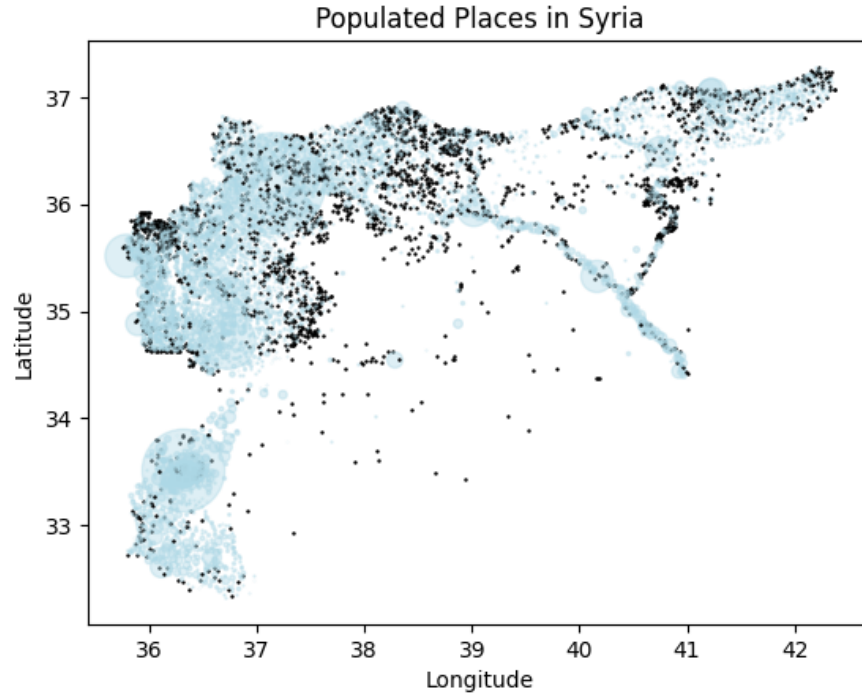


Figure 2. Map of Syrian populated places as catalogued by HOT (1). The bubble size signifies the relative population size, whereas black dots refer to places with no population data, assumed to be zero.

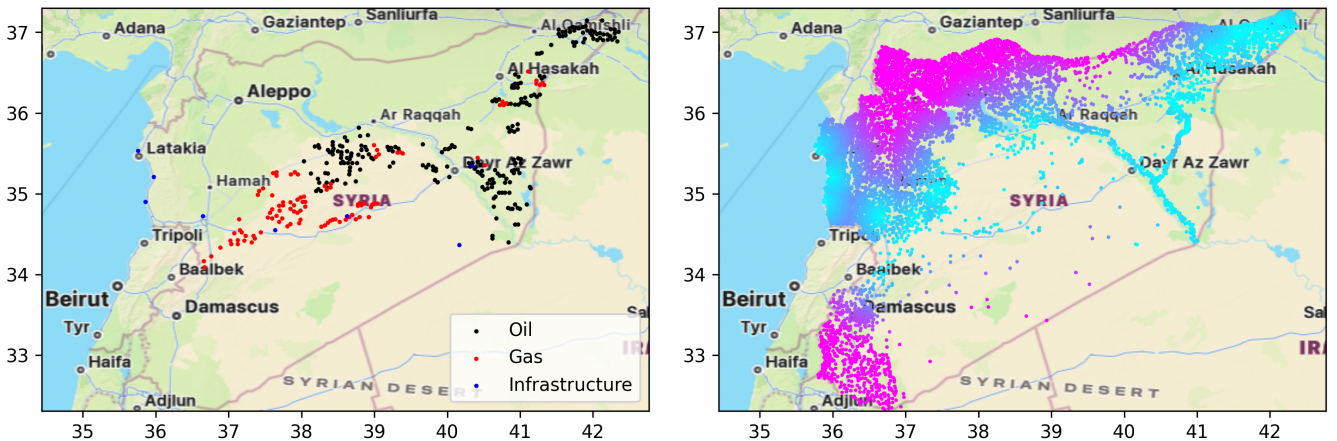


Figure 3. Left: Locations of oil reserves, gas reserves and important processing infrastructure obtained manually by maps in (2; 5). Right: Distance of the network's nodes to the closest point belonging to any of the three aforementioned categories. Light blue and magenta signify a small and large distance respectively.

It is also noteworthy that many of the largest Syrian cities contain a population large enough for these simplifications to potentially affect the course of the simulation nontrivially. For instance, even though Aleppo is taken to be Sunni-dominated, it is in reality a city where several groups coexist in comparable numbers: quoting from the [World Population Review](#), “The population [of Aleppo] consists of primarily of those of Arabic descent making up 59.2% of the overall population. Alawites make up 11.3% of the population and Levantines 9.3%. Kurds represent 8.9%, Druze 3.2%, Ismailis 2.1%, and Nusairis 1.3%”. These numbers if utilised in the troop-distribution process or the target selection of the simulation algorithm could affect the possession of a city which is of great strategic value for any party.

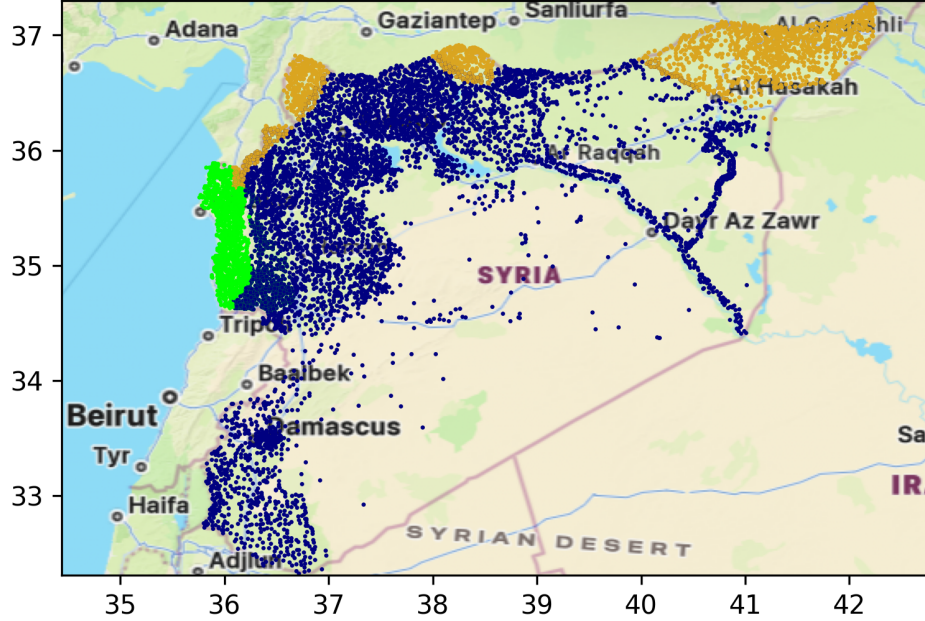


Figure 4. Nodes of the network colored by their dominant ethnoreligious group. Blue nodes carry the label *Sunni*, green nodes are *Alawites* and gold are *Kurds*, whereas nodes in overlap regions may carry more than one label.

3.4. Initial occupation state

The initial state of occupation concerning the ground controlled by the three parties is taken to be that of March 2019. The nodes are once more assigned an occupier based on regions drawn manually with no overlap, following a snapshot of the war from the YouTube video [Syrian Civil War and Spillover: Every Day](#) which illustrates a continuous visualisation of data collected from the sources in [this list](#). Evidently the process of data collection is not entirely reliable, nevertheless we consider the results, shown in 5, to be a sufficient approximation of reality for the purpose of providing an initial state for a dynamical simulation.

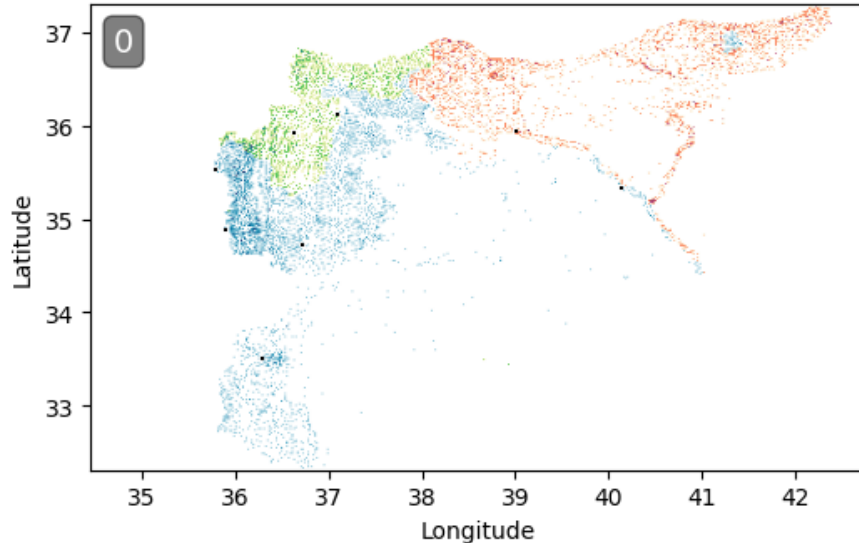


Figure 5. Initial state distribution of the different three factions as a heat map of the node distribution density. Blue denotes state-held nodes, green denotes Sunni-held nodes, and red denotes Kurd-held nodes. The black dots represent the location of major Syrian cities.

3.5. Centrality measures

The network's centrality measures are calculated using standard procedures and are assigned to each node as an additional trait. These measures highlight different structural properties of the network. Betweenness centrality quantifies the extent to which a node lies on the shortest paths between other nodes, thus identifying potential “bridges” or strategic intermediaries (Figure 6). Closeness centrality measures the inverse of the average shortest path from a node to all others, indicating how efficiently a node can reach or spread information across the network (Figure 7). Eigenvector centrality captures not only the number of connections a node has, but also their quality, assigning higher importance to nodes connected to other well-connected nodes (Figure 8). In particular, the raw values of eigenvector centrality were found to be extremely small, often clustered around machine-precision magnitudes. To avoid interpretative difficulties and to ensure that the measure could be meaningfully compared across nodes, we normalized eigenvector centrality. This normalization rescales the spectrum into a more manageable range, making differences in relative importance clearer while preserving the underlying structural ranking. In this way, the measure becomes more robust and interpretable, without altering its theoretical meaning.

In addition to these classical measures, the Fiedler value (the second smallest eigenvalue of the Laplacian matrix) was calculated to assess network connectivity and resilience. In order to focus the analysis on meaningful structural components, and evaluate the Fiedler value, the network was restricted to its largest connected sub-graph, excluding small disconnected fragments that do not contribute to the overall dynamics. Within this sub-graph, the measures were computed separately for the three main ethnic groups under study. This choice ensures that the reported values reflect the dominant structural properties of the system rather than noise introduced by marginal or sparsely connected components.

A small Fiedler value indicates weak algebraic connectivity, reflecting a network that can be easily partitioned or fragmented into communities. In our case, extremely small values on the order of 10^{-15} to 10^{-13} were obtained. These are within the range of floating-point numerical precision and may effectively represent zero. To address this, a threshold was introduced: only eigenvalues above a certain cut-off were considered as valid Fiedler values. This avoids misinterpreting numerical round-off errors as structural properties of the network. The values that we found are, for each ethnic community, at the given initial state distribution (Figure 5): $F_{Sunni} = 0.0453$; $F_{Kurds} = 0.00161$; $F_{State} = 0.000579$.

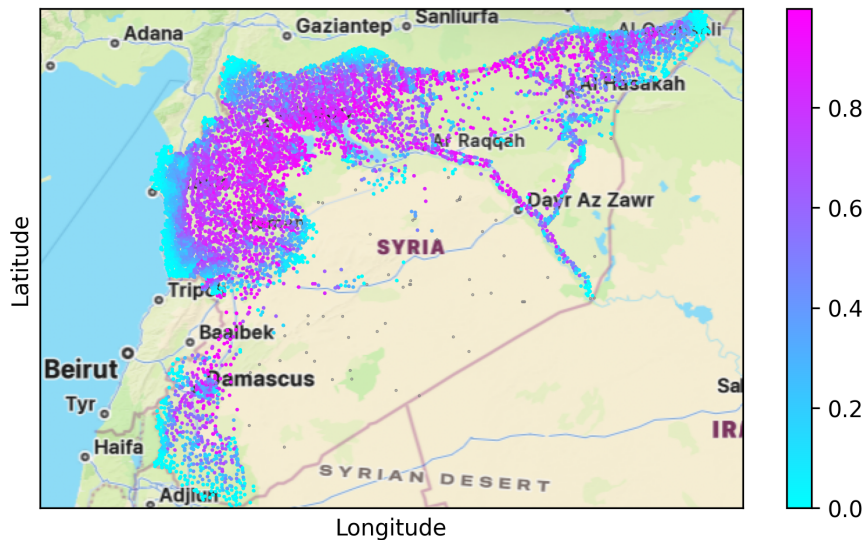


Figure 6. Betweenness centrality per node of the network. The colour value corresponds to $\frac{2}{\pi} \arctan(2000 \cdot bce)$ for given betweenness centrality bce .

4. RESULTS

In this paragraph we show different results that we obtained. We begin from the simplest iteration algorithm, then we show other notable results adding different network properties, and lastly a result using a different algorithm

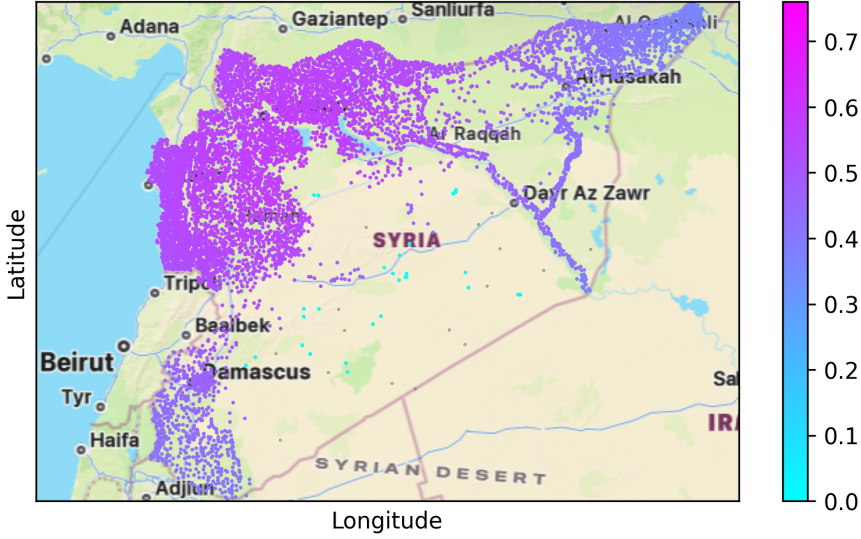


Figure 7. Closeness centrality per node of the network. The colour value corresponds to $\frac{2}{\pi} \arctan(25 \cdot cce)$ for given closeness centrality cce .

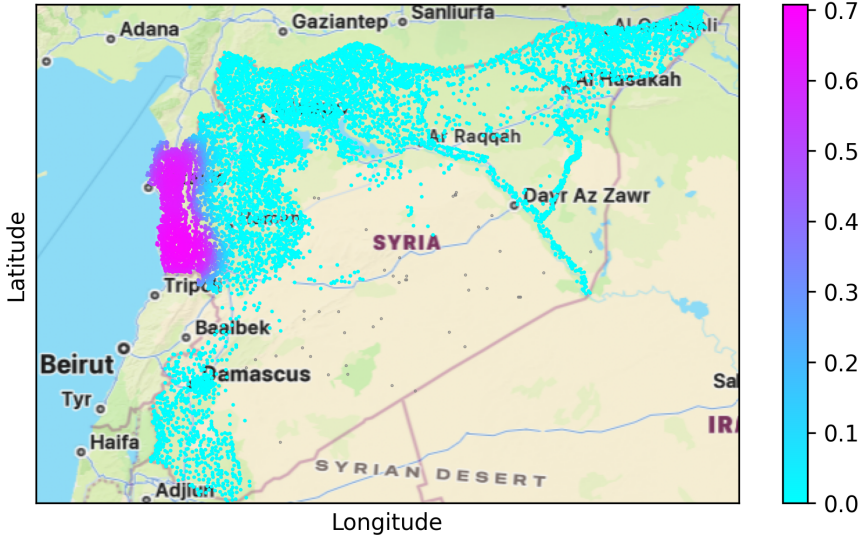


Figure 8. Normalized eigenvector centrality per node of the network. The colour value corresponds to $\frac{2}{\pi} \arctan(20 \cdot eig)$ for given eigenvector centrality eig .

that includes all the other network properties mentioned in the past section. All the simulations were initialized from the same occupation state depicted in Figure 5, allowing for direct comparison across algorithmic variants and network configurations. The results reveal that both the structure of the algorithm and the choice of network metrics significantly influence the evolution of territorial control and troop distribution.

All results are taken to represent the ultimate equilibrium reached by the simulation given a choice of parameters. That is because the simulation stops evolving significantly after a finite number of steps and is therefore cut at the 100th iteration, where we found that it has definitely reached an equilibrium phase where all changes are minor.

For the simulation parameters we set $\epsilon_{dist} = 0.3$, $c_{pop} = 0.01$, $c_{os} = 4.21$, $c_{dis} = 0.76$, $c_{ehtn} = 3$, $c_{bce} = 80$ for most applications unless stated otherwise. The network threshold distance is set at $d_0 = 0.1$ yielding the structure depicted in Figure 1.

4.1. Deterministic model: comparison of decision-making factors

The initial variant of the model, with purely deterministic target selection 2.1, was used to assess the impact of various parameters of the simulation that are associated with the decision-making process of the competing factions. In Figures 15, 16 we show respectively the end result of the simulation for choice of the c_{os}, c_{dis} parameters so that the maximal node for each case is assigned a probability 0.01 and 0.001, whereas the individual graphs correspond to the logical options AND-AND, (OR)-AND, AND-(OR), OR-OR.

The 0.01 and 0.001 thresholds serve to make the probability distributions less or more narrow, concentrated at small values. A smaller threshold would therefore mean that a town with a very small distance (from the attacker or from resources) would be considered significantly more important a target. Likewise, determining the logical combination of probabilities serves to hint at the mindset behind the most effective target selection: do we want towns that are nearby *and* big *and* close to resources, or maybe towns that are nearby *or* big *and* close to resources, or maybe...

We find that the most effective expansion for the Sunni rebels against the state is achieved using the AND-AND method with the looser option of the 1% parameters. This implies that the real turn of events in the war appears to emerge from a scenario where the factions place more importance to targets that feature several desirable traits simultaneously, although without being too strict when it comes to the individual traits. In general the system tends to produce rapid but brittle expansions, leading to overextension in peripheral regions. Ultimately we choose an AND-AND combination of probabilities and 1% parameters to proceed.

4.2. Model with stochastic target selection and memory

Another interesting, and different, result is given by (Figure 14), where the system evolves rapidly towards central hubs, leaning more towards Damascus, and focusing nodes with higher betweenness centrality. Moreover, in this case we can notice the absence of overextension in peripheral regions, as in (Figure 13). This is an important result, however not totally accurate, since the use of centrality measures led to a significant change in the simulation.

In contrast, the stochastic framework introduced in our Markov-inspired algorithm yields more gradual and adaptive dynamics. The probabilistic selection of targets, combined with mobility-weighted redistribution, allows factions to consolidate control in well-connected areas before expanding outward. Here, we present some result obtained with different strategies of modelling. The first, simplest, result is given by (middle right of Figure 17), as described in section 2.2 and 2.3, however omitting the structural collapse. This result shows how, for the chosen values, we're able to reproduce a quite rapid evolution from the "Sunni" nodes against the "State" ones, yet without reaching the Damascus node. This is a result of a pure network and stochastic model (the same result was achieved even adding the probability bias towards Damascus). Unlike deterministic formulations, this stochastic approach prevents the system from reaching a frozen equilibrium state. Essentially, each iteration includes probabilistic transitions weighted by both structural and contextual factors, there is always a non-zero probability of movement, ensuring continuous evolution. A more accurate result - in a strategical sense -, shown in Figure 17 (lower left), is obtained including the algorithm described in section 2.4. When the structural collapse mechanism is incorporated, the system exhibits accelerated transitions toward Damascus, one of the most important node in the network. This addition allows regions that have lost critical connectivity or strategic hubs to decay dynamically, triggering realistic cascades of territorial reorganization.

The inclusion of network centralities—such as eigenvector, closeness, and betweenness—proves critical in shaping both movement and strategic aggression. When these metrics are used in the mobility kernel, factions tend to reinforce hubs and corridors, resulting in resilient territorial clusters. When used in the attack probability distribution, they guide aggression toward structurally important nodes, accelerating the collapse of fragmented factions. A few examples are provided in Figure 17 where some observations can readily be made: betweenness, closeness and eigenvector centrality all yield a reasonable advance of the rebel factions into state-occupied territory which halts roughly at Homs, whereas there is more variety in the shape of the Sunni-Kurdish border along Euphrates.

Notably, simulations with betweenness centrality included in both movement and attack layers show the most realistic collapse patterns: factions that lose high-betweenness nodes suffer rapid fragmentation, while those that retain central corridors maintain cohesion. These outcomes align with observed strategic tendencies in real-world conflicts, where control of transit hubs and communication routes often determines operational success.

Overall, the results demonstrate that network-aware stochastic algorithms outperform simpler deterministic models in capturing the nuanced interplay between structure, strategy, and resilience in territorial dynamics.

Finally, a rather interesting result is given by a change of parameters in the memory-based algorithm (bottom right in Figure 17), that is going in (10) from 0.1% to 6% of the newly computed troops and 94% of previous troops. Here we can see the opposite result of what described previously, the evolution of "State" nodes against the "Sunni" nodes. This inversion arises with the increasing of the weight of newly computed troops (*new recruits*) enhances the reconstitution rate of the "State" faction's forces after each iteration. In practical terms, this means that nodes under government control continuously regenerate strength, compensating for territorial or structural losses more effectively. Consequently, the system becomes less dependent on historical charge accumulation (the memory term) and more responsive to the current territorial configuration.

From a modelling perspective, this behaviour represents a shift from inertia-dominated to reaction-dominated dynamics: when the recruitment term is stronger, the faction with higher population density or more centralized control — in this case, the "State" — gains a substantial advantage in sustaining or regaining lost ground. This effect can be interpreted as the emergence of a centralized logistical response, where supply and mobilization mechanisms compensate for earlier fragmentation.

Overall, this parameter change illustrates the sensitivity of the model to the balance between memory and renewal: a higher contribution of newly generated troops transforms the dynamics from long-term persistence of instability to a self-reinforcing recovery process dominated by centralized reorganization.

4.3. Parameter space exploration

In this section we perform a systematic parameter-space exploration to evaluate the sensitivity of our model to the coefficients c_{pop} , c_{os} , c_{dis} , and c_{bce} that enter the invasion kernel through the normalized expression $\arctan(cx)$, where $x \in [0, 1]$ represents the rescaled feature values of each node. All structural and socio-economic attributes—population, oil score, betweenness centrality, geographic distance, and adjacency—are normalized to ensure dimensionless comparability across different quantities. Each parameter pair is sampled logarithmically over several orders of magnitude (typically 10^{-2} to 10^6), providing a broad exploration of model behaviour.

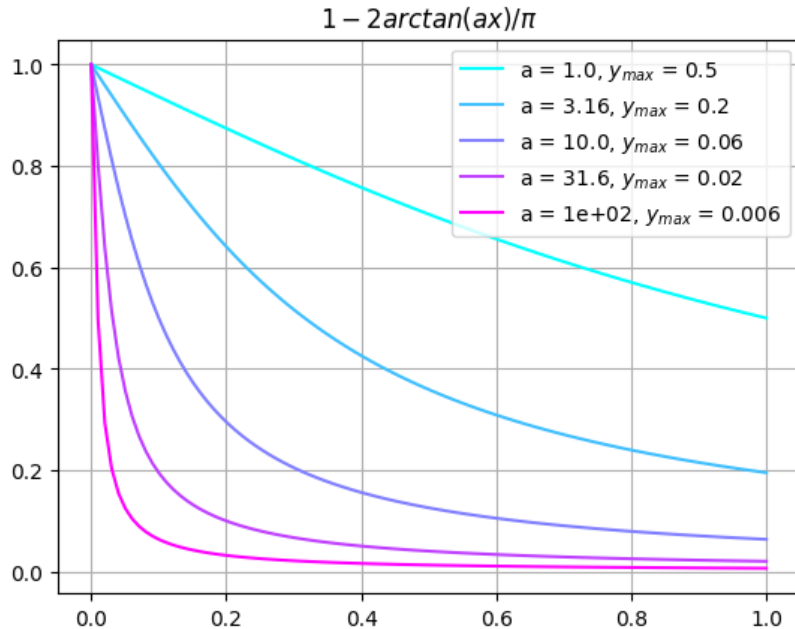


Figure 9. The model's normalised function $2 \arctan(ax)/\pi$ reflecting the value of a potential target as a function of a normalised feature x , for different values of the parameter a . High values of the parameter produce a steeper curve, which typically indicates a strictness in the underlying target evaluation process with respect to the feature x .

For each pair of parameters, we compute two complementary heatmaps showing the final fraction of occupied regions by the State and Sunni factions respectively, while the Kurdish-occupied fraction can be readily extrapolated. Each grid point corresponds to a full simulation run of 30 iterations, which were found enough to reach an equilibrium state,

where the network evolves according to the probabilistic invasion rules described in Section 2. As shown in Figure 10, the deterministic model exhibits relatively uniform outcomes across the explored parameter ranges. Furthermore, we observe that the parameters effectively decouple from each other in terms of how they affect the outcome of the simulation. For example, the value of c_{pop} for which the rebel occupation peaks comes out around 10^4 regardless of the parameter with which it is varied alongside. The red marker in each panel identifies the baseline configuration used throughout the main simulations, which is also used for the parameters that do not participate in the comparison of each heatmap.

The results indicate that, within the deterministic formulation, the model’s dynamics remain globally stable: the fraction of occupied regions does not vary drastically when either the population (c_{pop}) or oil-score (c_{os}) coefficients are perturbed within two or three orders of magnitude. This stability suggests that the deterministic invasion probabilities are dominated by the network’s structural connectivity, rather than by whether the evaluation of potential targets is strict or loose in terms of their desired features. This stable behaviour reaffirms the baseline configuration, confirming that the system captures the dominant topological dependencies between densely populated or resource-rich regions and their neighbouring nodes.

In an overview of our results we note the following trends: expansion of the rebel occupation is benefited by low values of c_{dis} and c_{os} , indicating a general indifference towards the proximity of the target and its proximity to oil and gas resources, and relatively high values for c_{pop} and c_{ethn} , signifying a preference for targets with large population and a matching ethnoreligious identity.

In contrast, when the same parameter-space analysis is repeated for the *memory-based algorithm* (Figure 11), the dynamics change considerably. In this extended formulation, each node retains a fraction of its previous charge distribution and redistributes it probabilistically according to a mobility kernel that depends on both distance and centrality measures. The memory term, as introduced in Equation (10), continuously updates the effective attack and movement probabilities, producing smoother transitions and a persistent capacity for motion even in quasi-equilibrium configurations.

A key quantitative difference is observed: in the memory-based model, the average occupied fraction for the State faction increases by approximately 0.20–0.25 compared to the deterministic case. This shift reflects the enhanced persistence and coordinated buildup of charge in central hubs, particularly around Damascus and other highly connected regions. Memory effectively acts as an endogenous reinforcement mechanism—territories that retain even a small charge fraction can regenerate local dominance over time, avoiding premature collapse. On the other hand, the same stochastic persistence also allows rebel factions to maintain long-term mobility and local influence, resulting in a richer, less abrupt evolution of territorial control.

The qualitative structure of the heatmaps further supports these interpretations. While the deterministic version (Figure 10) displays sharper transitions and relatively homogeneous regions, the memory-based one (Figure 11) exhibits more gradual gradients across the (c_{pop}, c_{os}) plane. This smoother morphology reveals a more adaptive dynamic regime, where competing effects such as population attraction, resource advantage, and geographic constraints balance continuously rather than discretely. Importantly, this regime avoids the “frozen” steady states occasionally observed in deterministic runs: due to the stochastic target selection and charge redistribution, there is always a finite probability of activation, preventing the system from reaching complete stagnation.

4.3.1. Discussion and theoretical implications

The parameter-space analysis plays a central role in assessing both the structural validity and the predictive robustness of our framework. Its purpose is threefold. First, it allows us to isolate the influence of each coefficient appearing in the invasion and mobility kernels, clarifying which mechanisms (population pressure, geographic distance, ethnic affinity, or network centralities) are dynamically dominant in driving territorial expansion. Second, by scanning each pair of parameters over wide logarithmic ranges, we can determine whether the model relies on delicate fine-tuning or whether its qualitative behaviour persists across broad regions of parameter space. Third, it provides an essential diagnostic tool for comparing deterministic and memory-based dynamics, enabling us to evaluate how the introduction of temporal feedback modifies the system’s long-term equilibrium.

The results indicate that the model is neither dominated by fine-tuning nor insensitive to its structural assumptions. By this we mean that, on one hand, small perturbations in the parameters do not radically alter the qualitative behaviour of the system (which would signal extreme fragility); on the other hand, parameter variations do produce systematic and interpretable changes, such as increases or decreases in territorial control that follow clear functional

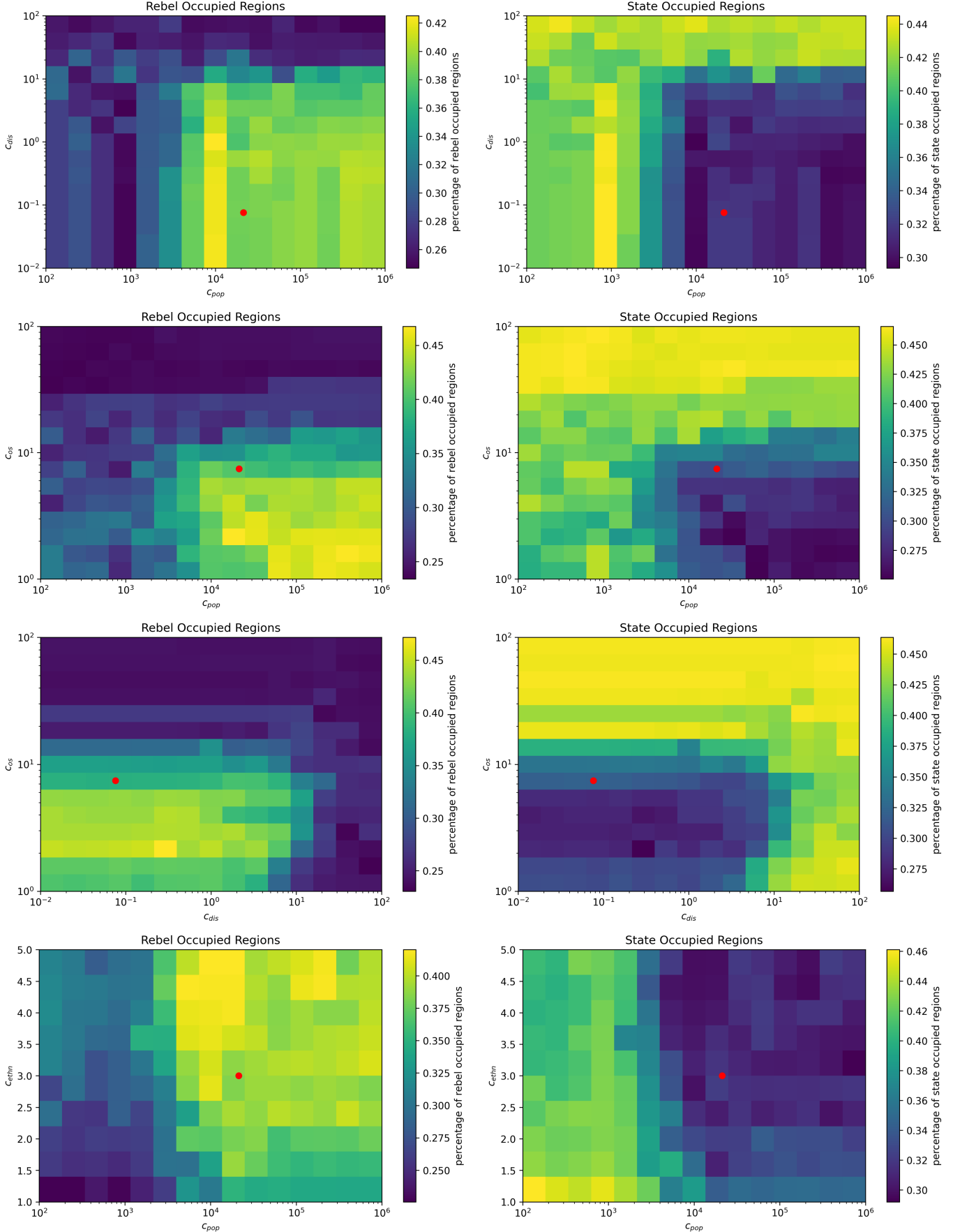


Figure 10. Parameter space exploration of c_{pop} , c_{dis} , c_{os} , c_{ethn} with the deterministic model running for 30 iterations per parameter choice. The red dot indicates the set of parameters used in the original simulation.

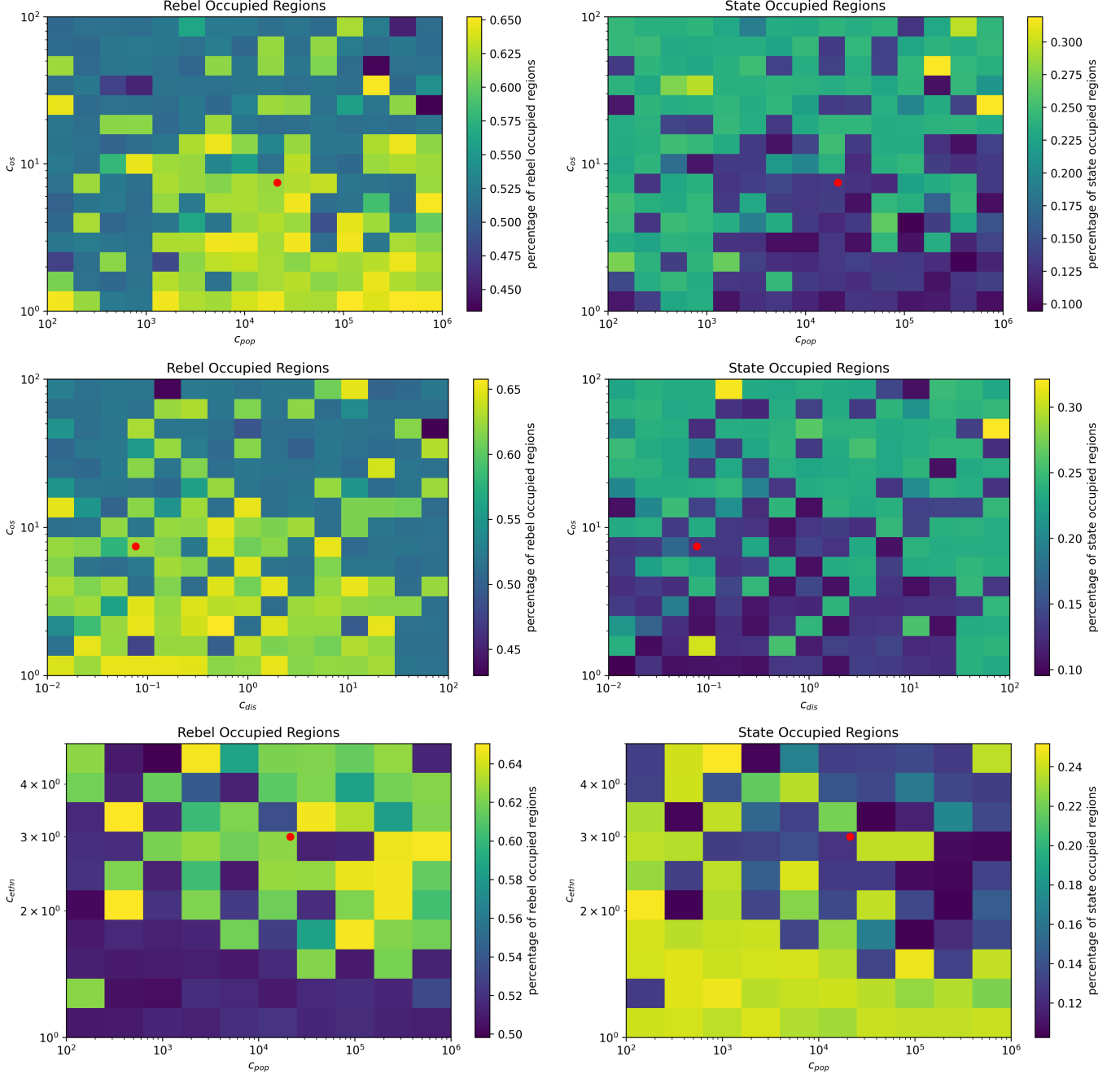


Figure 11. Parameter space exploration of $c_{pop}, c_{dis}, c_{os}, c_{ethn}$ with the memory-based model running for 30 iterations per parameter choice. The red dot indicates the set of parameters used in the original simulation.

trends. This balance is precisely what one expects from a physically meaningful model: it should be stable enough to allow interpretation, yet responsive enough to reveal the causal role of its internal mechanisms. The existence of coherent patterns across the heatmaps—for instance, the smooth gradients in occupation percentages and the roughly 20–25% shifts linked to stronger demographic or centrality-based weights—provides strong evidence that the model behaves in a controlled and theoretically intelligible way.

The parametric exploration also reveals a deeper conceptual distinction between the deterministic and the memory-based formulations of the model. In the deterministic scheme, evolution is entirely governed by the instantaneous maximisation of invasion probabilities. This leads to dynamics that tend toward fixed or cyclic configurations, often

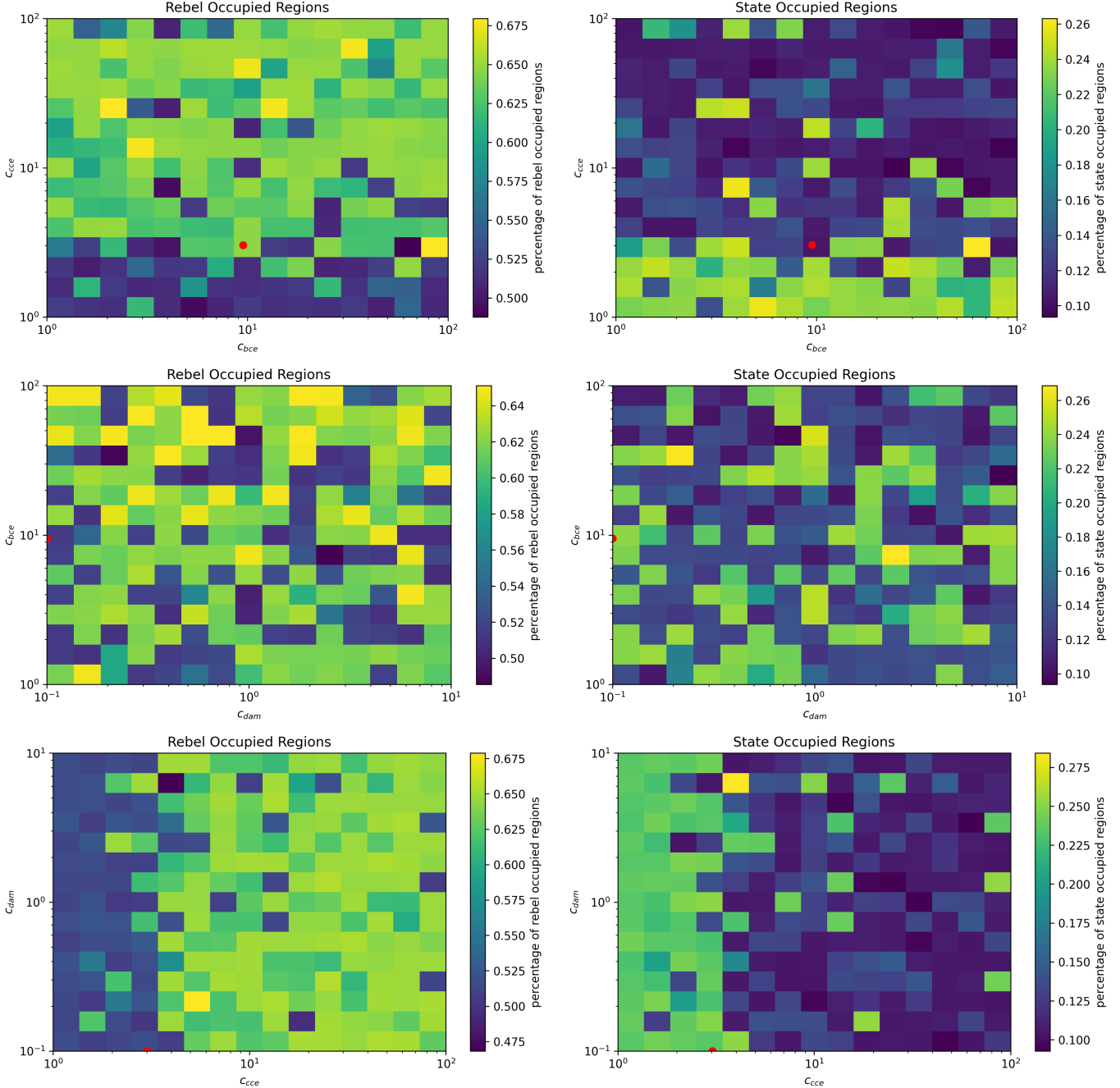


Figure 12. Parameter space exploration of c_{bce} , c_{cce} , c_{dam} with the memory-based model running for 30 iterations per parameter choice. The red dot indicates the set of parameters used in the original simulation.

becoming trapped in local maxima where no faction possesses sufficient incentive or capacity to advance further. As a result, stagnation phases emerge naturally: the system can settle into patterns where territorial fronts remain static, and long-term reorganisation becomes extremely unlikely.

The memory-based model, by contrast, introduces a non-Markovian feedback mechanism that fundamentally changes the nature of the dynamics. Here, the redistribution of charges is influenced not only by the current state of the network but also by the accumulated history of troop flows. This transforms the fixed network into a temporally evolving weighted structure, in which effective edge strengths emerge from past mobility and territorial exchanges. From a network-theoretic perspective, this corresponds to a first-order temporal extension of the static graph: transitions are

no longer determined solely by local topology but by a path-dependent combination of geometric, demographic, and historical factors. The memory mechanism therefore acts as an adaptive stabiliser, continually reinforcing strategic corridors and mitigating short-term losses.

These differences manifest clearly in the parameter-space maps. When memory is active, the system avoids long-term stagnation: even in regions of parameter space where deterministic dynamics stall, the probabilistic reinforcement of successful trajectories ensures that some direction of motion remains available. This not only accelerates the collapse of fragmented factions but also increases the overall territorial footprint of successful groups. The observed 20–25% increase in occupied regions under memory-based rules demonstrates the self-reinforcing nature of adaptive mobility: once early successes occur, they propagate through the charge redistribution mechanism, amplifying strategic advantages over time. Such behaviour is not an artefact of specific parameter choices but emerges consistently across broad swaths of the parameter space, as the maps indicate.

In conclusion, the parameter-space analysis provides a comprehensive validation of the model. It shows that the deterministic formulation captures essential competitive interactions but is limited by its lack of temporal adaptation, while the memory-based model introduces a realistic mechanism for cumulative strategic advantage. More broadly, the analysis demonstrates that our framework remains coherent across large ranges of parameters, that its qualitative outputs are not the result of narrow fine-tuning, and that the introduction of stochastic memory significantly enhances its expressive power. Altogether, these results give the model a solid theoretical foundation: they show how local interactions, global topology, and temporal feedback combine to produce macroscopic patterns of territorial expansion, resilience, and collapse, providing insights that are both robust and conceptually meaningful.

5. CONCLUSIONS

Evidently our treatment did not involve factors that relate in any way to external support, such as funding, shipment of weapons or bombing – even though these were factors of decisive importance throughout the war’s duration. Nevertheless, when these factors were effectively ultimately removed to a large extent, the inert situation in Syria was allowed to progress under the influence of internal driving forces, the effect of which we expect to observe in our results. The simulations thus allow for some educated speculation into the dynamics that drive the war’s evolution, especially in significant turning points such as the sudden takeover of the state-held territory by the rebel groups.

Our choice of parameters was generally governed by their ability to reproduce the victory of the Sunni rebels over the Syrian state’s army, nonetheless it is remarkable that in most of our various attempts the situation for the rebels was either inert or favourable, but not adverse. This may be attributed to our choice to place weight on the support by the dominant ethnic or religious group, as the Sunni takeover occurs mostly in a Sunni dominated region. All the while, as was discussed in the results section, the most effective choices of parameters and logical approach indicate that the three factions prefer to select targets that carry several positive traits simultaneously, with a moderate strictness towards the individual traits. This assessment could be improved by examining different decision-making processes for different factions.

In performing a search of our parameter space we come to understand that adjusting the strictness of the target evaluation procedure, encoded in the various c parameters that control the steepness of the respective probability-like functions, does not influence the aforementioned observations significantly as the general tendency of the rebel territory to expand at the expense of state territory persists. The fraction of occupied territory, although changing marginally in the initial simulation algorithm, can nevertheless be seen to rise significantly when the more realistic, memory-based algorithm is implemented. Ultimately, the central takeaway from the parameter space searches is that the rebel advance is favoured by a target selection process that is strict when it comes to large population and matching of the ethnoreligious identity, and comparatively relaxed when it comes to vicinity to energy resources and infrastructure and vicinity to the attacker. Furthermore, closeness centrality appears to be the more distinctly favourable centrality measure to the rebel advance compared to betweenness centrality.

At the same time, it is impressive that the Kurdish territory remains for the biggest part unaffected, with its resulting borders following roughly the river Euphrates, the presence of which was not explicitly modelled into the simulation, but which indeed became the natural border between the new Syrian state, the product of the Sunni takeover, and the Kurdish territory. Even though its south and east parts do not see much activity in the simulation because they belong to poorly connected areas of the network, bordering regions that are very sparsely populated, its northwest part lies in a wide region of strongly connected nodes and therefore is invisible to the simulation’s dynamics. Nonetheless, ultimately we are able to recover the real outcome of two surviving factions, Sunni and Kurds, separated by the river.

Other potential scenarios, like the takeover of the Sunni territory by state troops, are also found to be possible, though generally less likely, results if the parameters of the simulation are adjusted favourably.

We conclude that the dynamics of the conflict, although impossible to fully understand without the inclusion of several additional parameters of, for instance, geopolitical or financial nature, are at times guided to an important extent by simple underlying parameters - the support of the local population, the vicinity to valuable resources, the accessibility and connectivity of a location, all are qualities which affect the activity of the competing factions. A simulation like the one performed in this work may thus make a naive guess as to how a conflict might proceed to potentially unexpected results, when external factors diminish and leave it to its own devices.

REFERENCES

- [1] Syria Populated Places (OpenStreetMap Export),
Humanitarian OpenStreetMap Team (HOT).
https://data.humdata.org/dataset/hotosm_syr_populated_places.
Alternatively <https://tinyurl.com/47rr3jmm>.
- [2] Syrian Oil and Gas, The Energy Consulting Group:
Management consultants for upstream oil and gas
producers and service companies.
<https://www.energy-cg.com/MiddleEast/Syria/Syria>
- [3] Demographics, Heritage For Peace.
<https://www.heritageforpeace.org/syria-country-information/geography/>.
- [4] Syria, Minority Rights Group.
<https://minorityrights.org/country/syria/>.
- [5] Brenda Shaffer. Syria's energy sector and its impact on
stability and regional developments, Atlantic Council, 17
Jan 2025. <https://www.atlanticcouncil.org/in-depth-research-reports/issue-brief/syrias-energy-sector-and-its-impact-on-stability-and-regional-developments/>.

6. APPENDIX

In this appendix, we report the outcomes of the evolution algorithm described in the main text. These graphical outputs complement the dynamic discussed earlier. Some of our results, including what was presented in this work, will be made available in [this GitHub repository](https://github.com/KonTopal/Syria_war) (github.com/KonTopal/Syria_war) in picture and mp4 format, along with the relevant code and data.

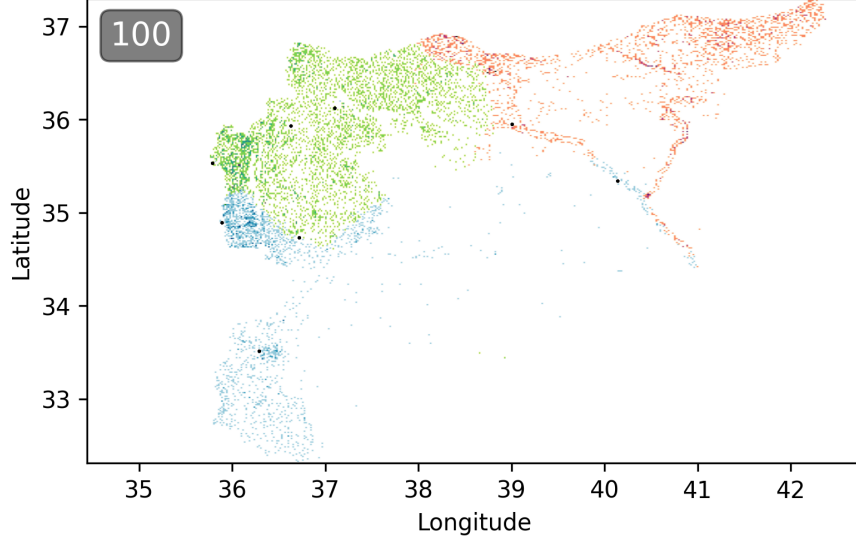


Figure 13. Final state distribution of the different three factions. This graph is a result of the plain iteration algorithm, as described in 2, without using any network measure.

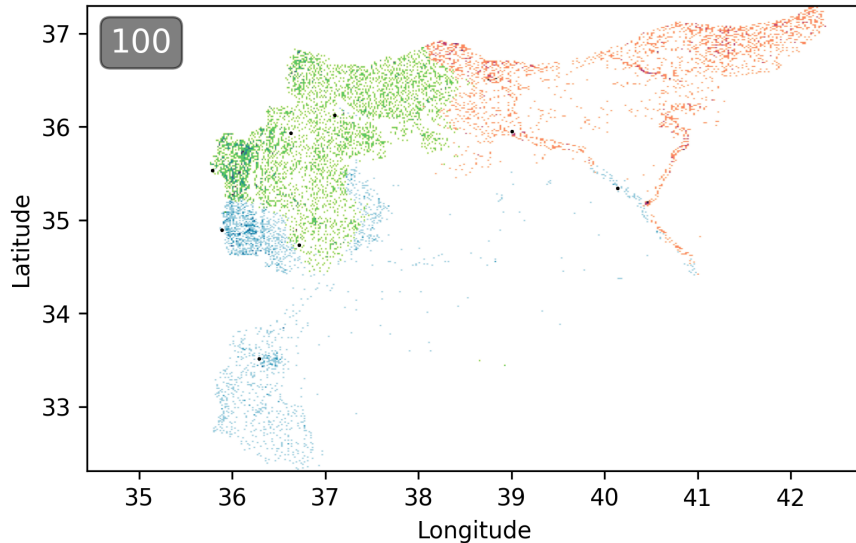


Figure 14. Final state distribution of the different three factions. This graph is a result of the iteration algorithm, as described in section 2.1.

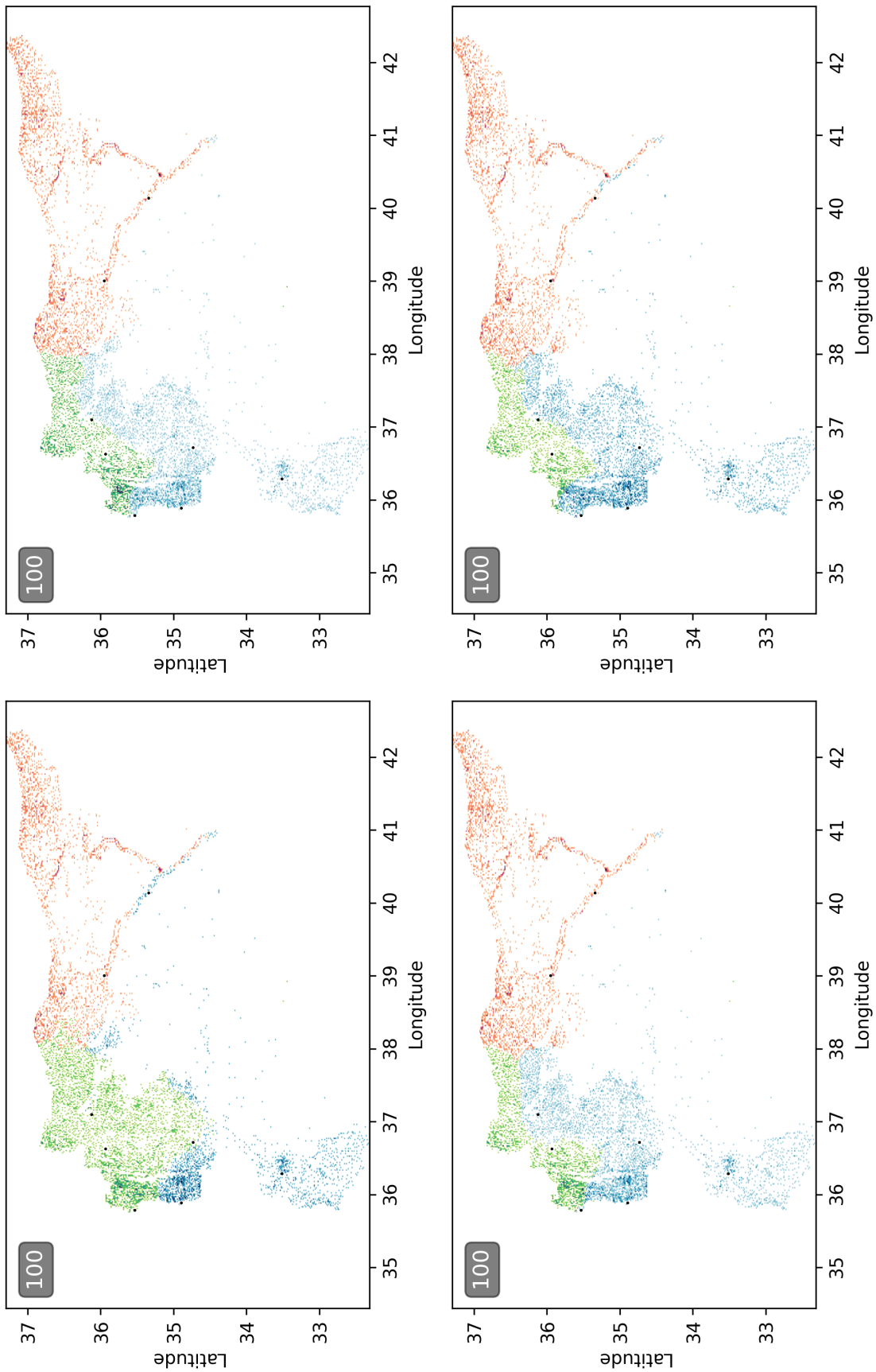


Figure 15. Results of the simulation for different logical decision-making approaches. Upper left: AND-AND. Upper right: OR-OR. Lower left: AND-(OR). Lower right: (OR)-AND. The parameters $c_{os} = 4.21$, $c_{dis} = 0.76$ correspond to a 1% threshold.

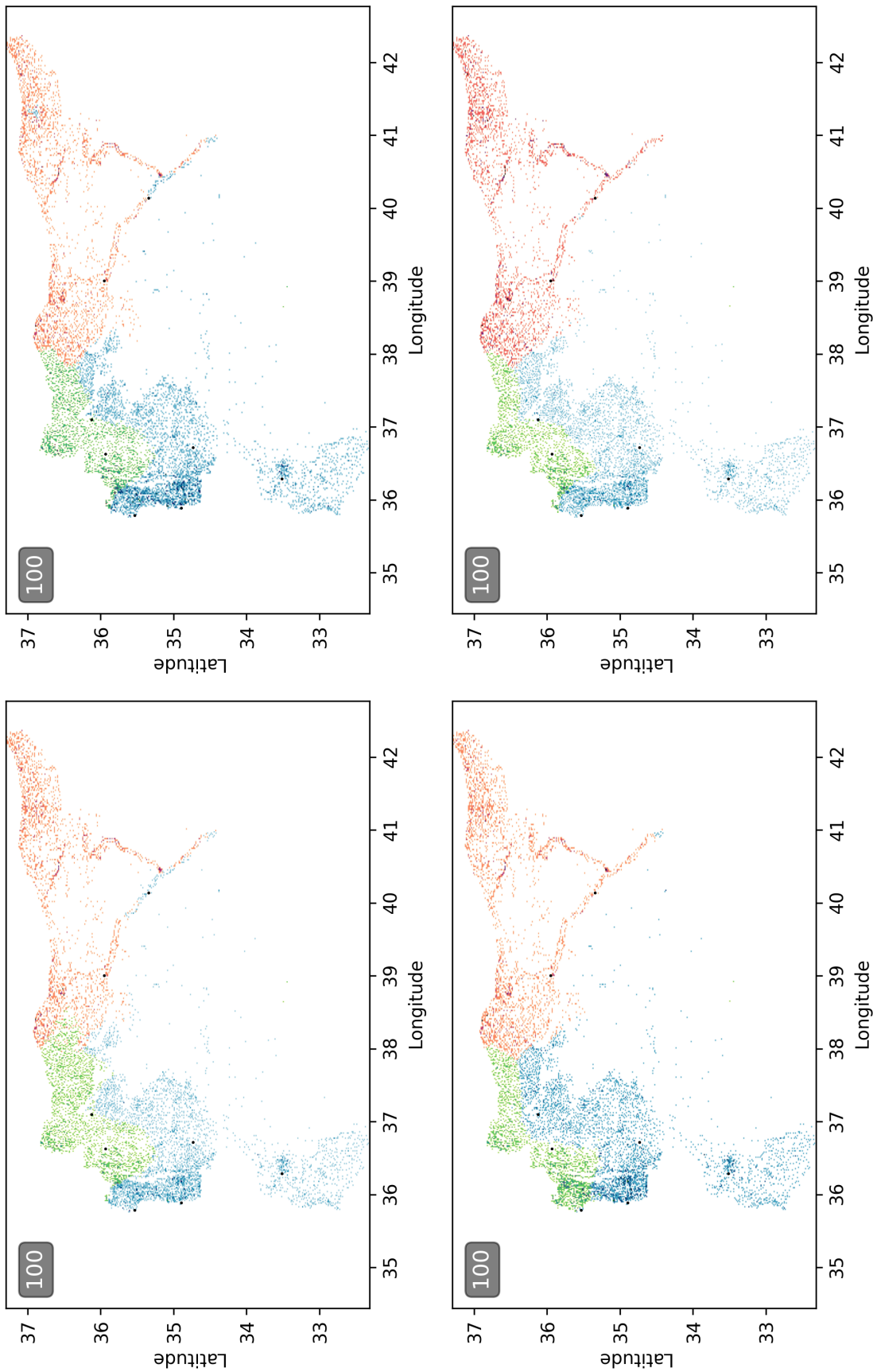


Figure 16. Results of the simulation for different logical decision-making approaches. Upper left: AND-AND. Upper right: (OR)-AND. Lower right: OR-OR. The parameters $c_{os} = 42.22$, $c_{dis} = 7.67$ correspond to a 0.1% threshold.

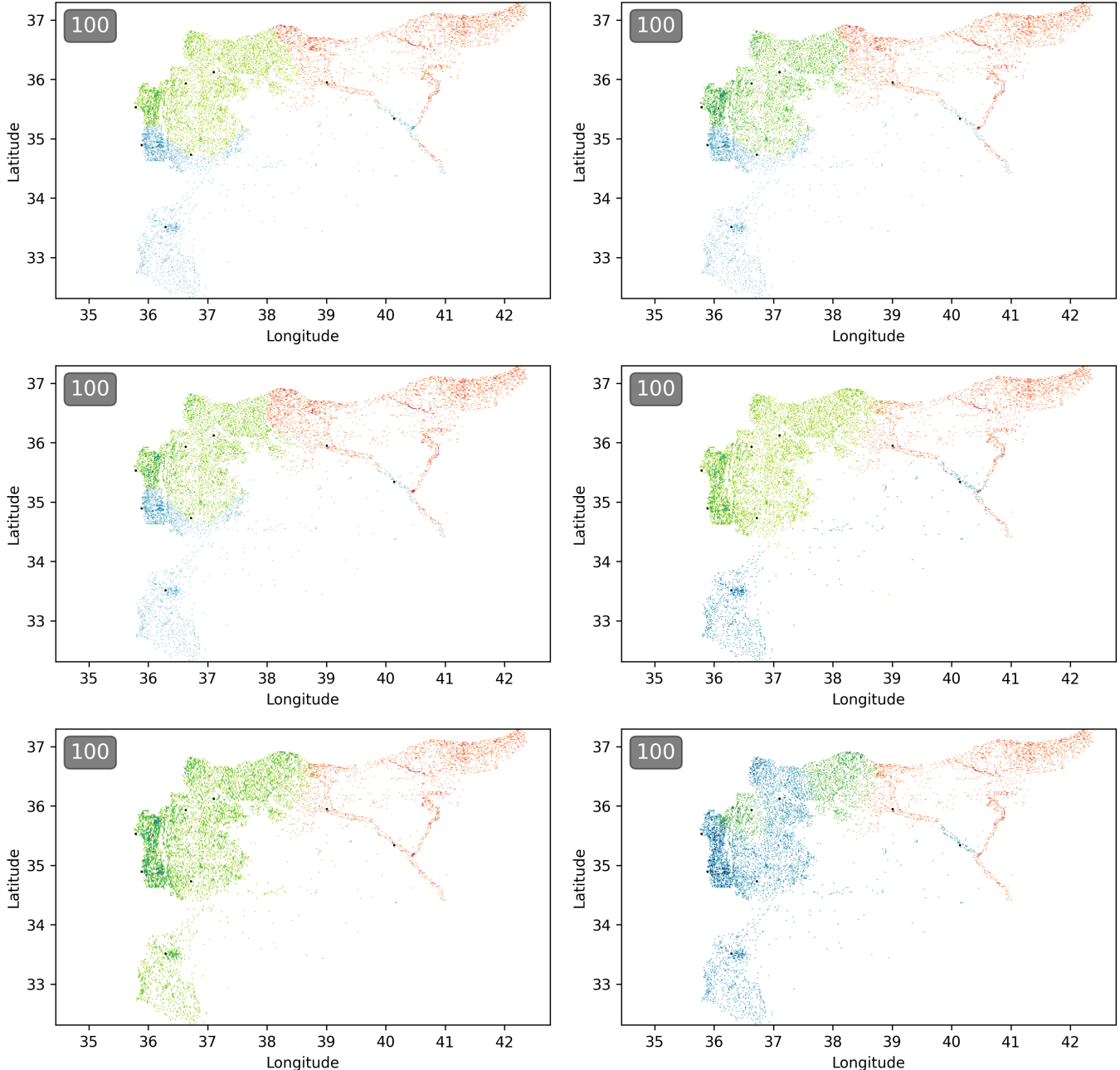


Figure 17. Final state distribution of the different three factions with different simulation parameters. (upper left) Only closeness centrality incorporated. (upper right) Closeness centrality and distance from Damascus parameter. (middle left) Eigenvector centrality and distance from Damascus parameter. (middle right) Stochastic algorithm, as described in the sections 2.2, 2.3, without considering the bias probability towards Damascus. (lower left) Stochastic algorithm, as described in the sections 2.2, 2.3, 2.4. (lower right) Stochastic algorithm, as described in the sections 2.2, 2.3, with modified algorithm weights.

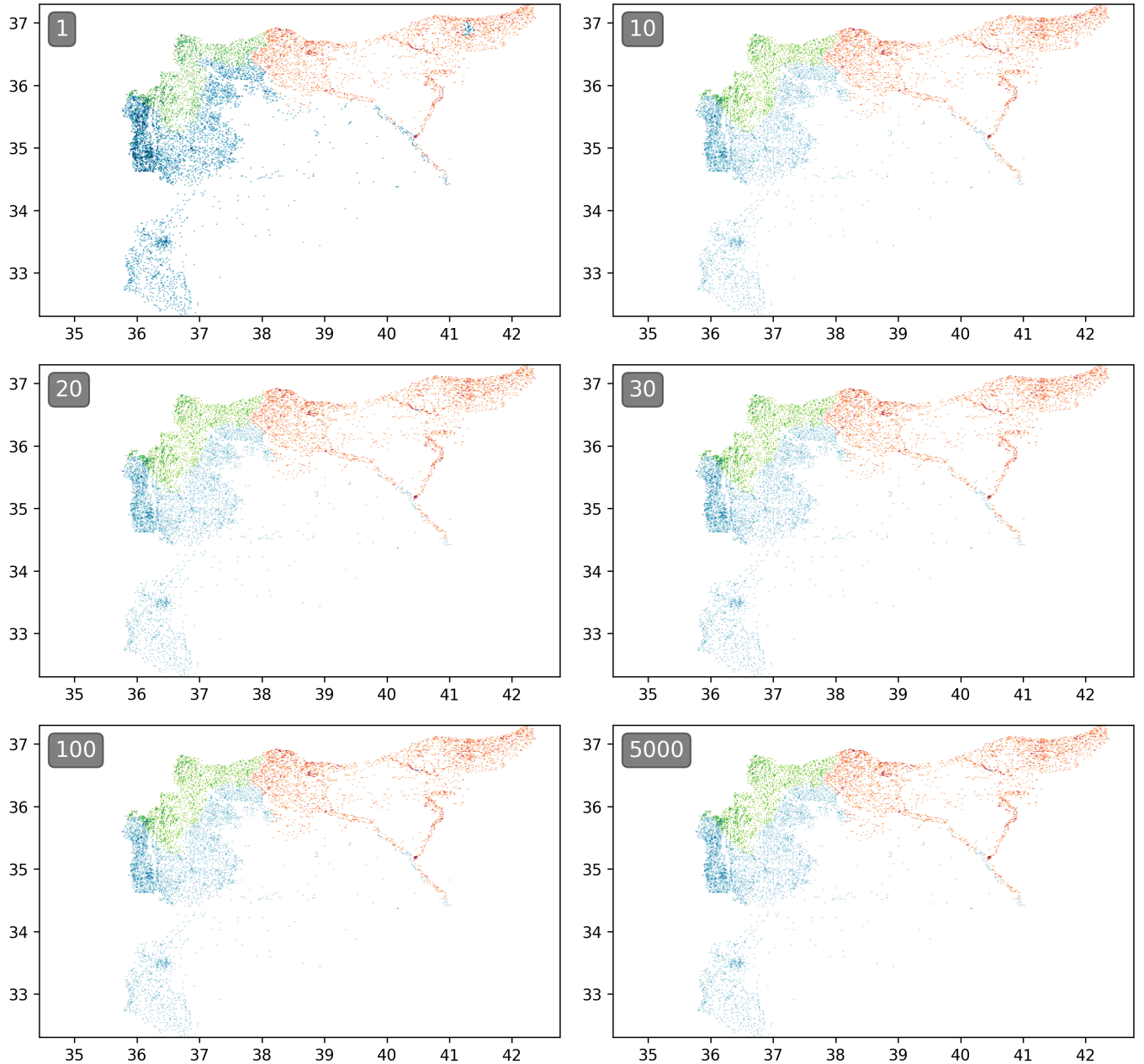


Figure 18. Course of the simulation over a large number of iterations (non-stochastic OR-OR algorithm without centrality parameters). The simulation evolves the initial configuration in the first few iterations, and remains inert after achieving an equilibrium. We henceforth regard $N=100$ as a sufficient number of iterations for any algorithm.